

## Probing the adhesion of submicron thin films fabricated on a polymer substrate via nano-transfer printing

This article has been downloaded from IOPscience. Please scroll down to see the full text article.

2012 J. Micromech. Microeng. 22 095002

(<http://iopscience.iop.org/0960-1317/22/9/095002>)

View [the table of contents for this issue](#), or go to the [journal homepage](#) for more

Download details:

IP Address: 115.170.244.239

The article was downloaded on 27/07/2012 at 09:20

Please note that [terms and conditions apply](#).

# Probing the adhesion of submicron thin films fabricated on a polymer substrate via nano-transfer printing

Andy Fox<sup>1</sup>, D R Hines<sup>2,4</sup> and Teng Li<sup>1,3,4</sup>

<sup>1</sup> Department of Mechanical Engineering, University of Maryland, College Park, MD, 20742, USA

<sup>2</sup> Laboratory for Physical Sciences, College Park, MD, 20740, USA

<sup>3</sup> Maryland NanoCenter, University of Maryland, College Park, MD, 20742, USA

E-mail: [LiT@umd.edu](mailto:LiT@umd.edu) and [hines@lps.umd.edu](mailto:hines@lps.umd.edu)

Received 19 March 2012, in final form 14 June 2012

Published 26 July 2012

Online at [stacks.iop.org/JMM/22/095002](http://stacks.iop.org/JMM/22/095002)

## Abstract

Determining the interfacial adhesion of ultrathin functional films in micro-electro-mechanical systems (MEMS) and nano-electro-mechanical systems (NEMS) becomes increasingly crucial for optimal design of MEMS/NEMS devices. However, direct measurement of adhesion properties of ultrathin films can be challenging, as the traditional metrology of adhesion at macroscopic scales becomes unsuitable in dealing with samples of extremely small dimension. In this paper, we present a feasible and robust approach combining nano-transfer printing (nTP) experiments and mechanics modeling to quantitatively determine the interfacial adhesion of submicron thin films. We show that the measurements of the interfacial adhesion of a submicron polycarbonate (PC) thin film on a PC substrate at multiple locations in multiple samples agree within 7.3%, demonstrating the accuracy and robustness of our approach. Given the versatility of the nTP process, the approach demonstrated in this paper is expected to be generally applicable to measure the adhesion of interfaces of other material combinations. In this sense, this study sheds light on better understanding of the adhesive properties of functional interfaces in MEMS and NEMS.

(Some figures may appear in colour only in the online journal)

## 1. Introduction

The potential impact of micro-electro-mechanical systems (MEMS) and nano-electro-mechanical systems (NEMS) on modern technology and science cannot be overstated [1–4]. As the feature sizes of MEMS and NEMS continuously decrease, the role of surfaces and interfaces in miniaturized devices becomes increasingly crucial in the material selection and structural optimization of MEMS and NEMS to achieve desired functions [1, 5, 6]. One particular challenge to the future success of MEMS and NEMS technology is to precisely determine the interfacial adhesion between ultrafine scale materials (e.g. submicron thick functional thin films). Direct measurement of such interfacial adhesion properties of ultrathin films is challenging, as the traditional metrology

of adhesion at macroscopic scales (e.g. peeling tests, wedge tests, or double-cantilever beam methods) becomes unsuitable in dealing with samples of extremely small dimension [6, 7]. On the other hand, if the interfacial adhesion between various thin film materials can be well understood and furthermore better controlled, it enables novel micro-/nano-fabrication approaches for MEMS and NEMS. For example, nano transfer printing (nTP) [8–13] is a nanofabrication technique that involves an assembly process by which a thin printable layer can be transferred from a transfer substrate to a device substrate. nTP mainly relies on the differential interfacial adhesions between the thin printable layer and the transfer/device substrates, and thus allows for printing a wide range of functional thin film materials onto unconventional device substrates (e.g. polymers and elastomers). As a result, nTP is emerging as a potential fabrication technique to enable a low-cost and scalable roll-to-roll printing process for the

<sup>4</sup> Author to whom any correspondence should be addressed.

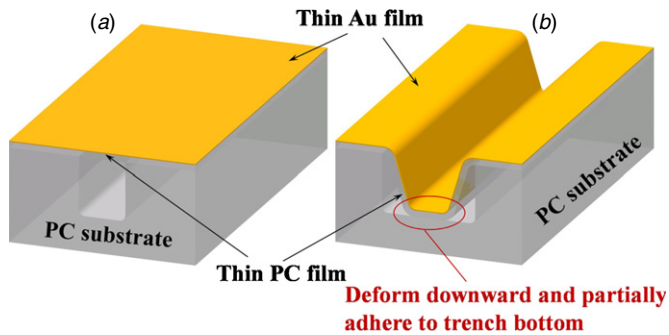


**Figure 1.** (a) An Au/PC bilayer can be suspended over a long trench of moderate width on a PC substrate. (b) If the trench is too wide, the Au/PC bilayer can deform downward and adhere partially to the bottom of the trench (not to scale).

fabrication of flexible devices [14–16]. The quality of nTP hinges upon the precise control of the differential interfacial adhesions, which is so far mainly achieved via trial-and-error [12]. Therefore, a quantitative approach to determining the interfacial adhesion of ultrathin films is highly desirable. To address this concern, we report an approach combining nTP experiments and mechanics modeling to quantitatively determine the interfacial adhesion of submicron thin films of polycarbonate (PC) fabricated on a PC substrate via nTP. Given the versatility of the nTP process, the approach demonstrated in this paper is expected to be generally applicable to measure the adhesion of interfaces of other materials combinations. In this sense, results from this study shed light on better understanding of the adhesive properties of functional interfaces, which in turn help guide the optimal design of MEMS and NEMS.

This study is inspired by our recent efforts to fabricate thin-film nano-resonators using nTP [17]. In such a nano-resonator, a thin Au film (30 nm thick) deposited on a thin PC film (900 nm thick) is suspended over a long trench in a PC substrate (similar to figure 1(a) but with an Au electrode previously printed into the bottom of the trench). The Au/PC bilayer can be mechanically excited when the frequency of the AC voltage applied to the top and bottom Au electrodes of the nano-resonator reaches the resonant frequency of the Au/PC bilayer. During the nTP fabrication of the nano-resonators (to be detailed in section 2), we find that the Au/PC bilayer can be successfully suspended over trenches of small and moderate widths (e.g. less than 100  $\mu\text{m}$ ) (figure 1(a)); however, if the cavity width is too large, the Au/PC bilayer tends to deform downward and partially adhere to the bottom of the trench (figure 1(b)). A similar phenomenon is also observed when a thin PC monolayer is transfer printed over the trenches on a PC substrate with various widths. As to be detailed in section 3, the deforming and adhering of the Au/PC bilayer (or the PC monolayer) onto the trench bottom is dictated by the energetic competition between the interfacial adhesion of the thin PC film and the PC substrate and the elastic energy of the Au/PC bilayer (or the PC monolayer) due to downward deformation. Based on such an energetic competition, a mechanics model is devised in section 3 to determine the critical conditions of partial adherence formation. Combining model analysis with experimental measurement of the deformed profile of the

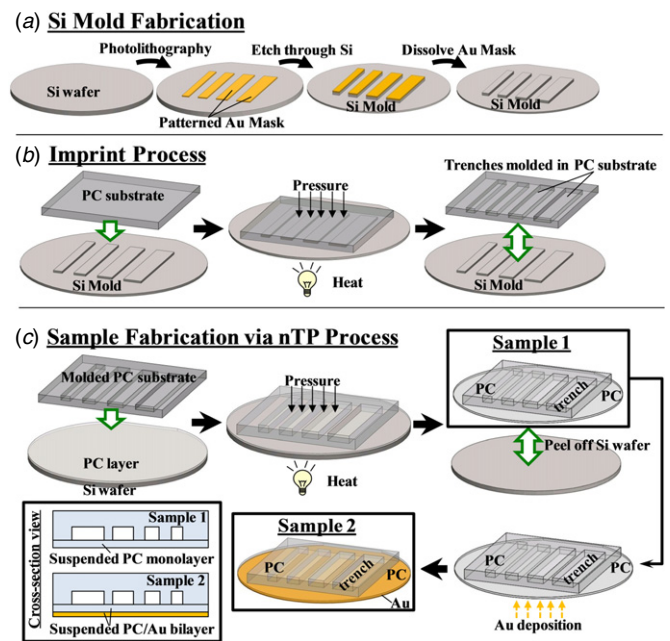


**Figure 2.** Illustrations of (a) Si mold fabrication, (b) trench imprinting process in PC substrate, and (c) final sample fabrication via nTP process.

Au/PC bilayer (or the PC monolayer), the interfacial adhesion between a submicron thin film of PC and the PC substrate can be quantitatively determined.

## 2. Sample fabrication and characterization

Figure 2 illustrates the experimental procedures used to fabricate the samples illustrated in figure 1. First, a pattern of 1 cm long strips of 500 nm thick Au with various widths from 4 to 2000  $\mu\text{m}$  is fabricated on the surface of a Si wafer using standard photolithography with negative photoresist, e-beam metals deposition and lift-off. The Au pattern is used as an etch mask to create 8  $\mu\text{m}$  high Si mesas by reactive ion etching of the Si wafer to remove the portion of the wafer that is not covered by the Au mask. The Au mask is then dissolved from the Si wafer.<sup>5</sup> Next, the resulting Si mold is used to imprint trenches of various widths into a thick PC substrate in a Nanonex NX2500 nanoimprinter at 170  $^{\circ}\text{C}$  and 500 psi for 3 min (figure 2(b)). Finally, a thin layer of PC (900 nm thick) is spun coated on a second (unpatterned) Si wafer and then brought in contact with the molded PC substrate in the Nanonex NX2500 nanoimprinter with a temperature of 140  $^{\circ}\text{C}$  and pressure of 500 psi and for 3 min (figure 2(c)). After cooling down and releasing pressure, the Si wafer is peeled off. The resulting structure (referred to as sample 1 hereafter) includes a thin PC film covering all the previously printed cavities in the PC substrate. If necessary, a thin layer of Au (30 nm) can be deposited on the top surface of the thin PC

<sup>5</sup> To fabricate the aforementioned nano-resonators, the Au mask is left on the surface of the Si mesas and then transfer printed to the bottoms of the resulting imprinted trenches in the PC substrate. For all samples in the present paper, the Au mask is removed from the surface of the Si mesas.

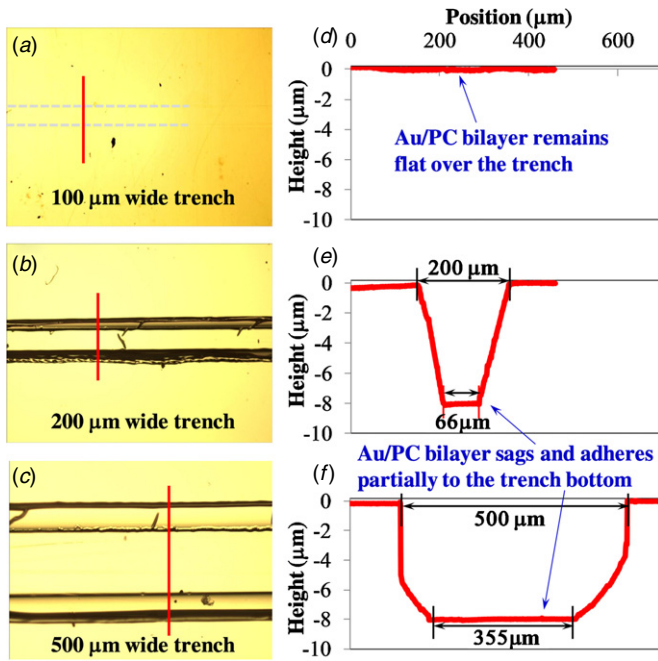


**Figure 3.** (a)–(c) Close-up optical images of the regions in sample 2 where the Au/PC bilayer covers trenches of width of 100 μm, 200 μm and 500 μm, respectively. The dashed lines in (a) highlight the edges of the underlying trench. Surface profile scanning of the Au/PC bilayer over the trench are performed along the vertical solid lines shown in (a)–(c), which are plotted in (d)–(f), respectively. Au/PC bilayer remains flat over the 100 μm wide trench, but deforms downward and adheres partially to the bottom of the 200 μm and 500 μm trenches, with a width of adhered portion of 66 μm and 355 μm, respectively.

film, resulting in the sample as illustrated in figure 1 (referred to as sample 2 hereafter).

Figures 3(a)–(c) show close-up optical images of the regions in sample 2 where the Au/PC bilayer covers trenches of width of 100 μm, 200 μm and 500 μm, respectively. The smooth Au surface as shown in these images suggests negligible residual stress due to thermal mismatch during fabrication. Over a narrow trench (of width equal or less than 100 μm), the Au/PC bilayer remains flat and suspended freely. Over a wider trench (of width equal or greater than 200 μm), the Au/PC bilayer deforms downward and adheres partially to the bottom of the trench. For example, 3D surface profile scanning of the Au/PC bilayer over the trenches via a Veeco interferometric microscope reveals that the widths of the adhered portion of the Au/PC bilayer over the 200 μm and 500 μm wide trenches are 66 μm and 355 μm, respectively (figures 3(e) and (f)). The height difference of the scanning of the Au surface is equal to the trench depth (8 μm), indicating that no delamination occurs between the Au/PC interface during the nTP process. All trenches in our samples are of length of 11 mm. To avoid the edge effect, all measurements are taken in regions that are far away from the two opposite ends of each trench. A similar phenomenon is also observed in sample 1. For example, the PC monolayer remains flat and suspended over trenches of width equal or less than 100 μm but deforms down and partially adhere to the bottom of trenches of width equal or greater than 200 μm.

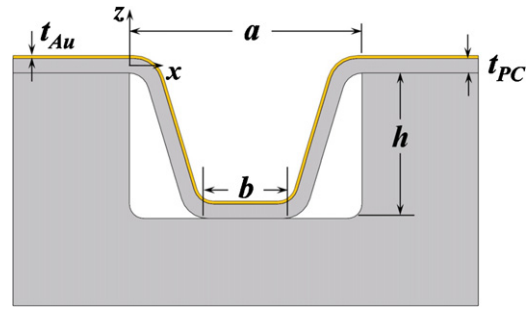


**Figure 4.** Schematic of the cross-section view of the Au/PC bilayer deforming and partially adhering to the trench bottom (not to scale).

### 3. Mechanics model and results

In this section, we delineate a mechanics model to decipher the energetic interplay that governs the resulting morphology of the Au/PC bilayer (or the PC monolayer) over trenches of various widths. Figure 4 defines the key geometric parameters of the Au/PC bilayer and the trench. There are existing models dealing with the adhesion-delamination mechanics of a suspended layer over a trench emphasizing various effects of residual stress, long-range electrostatic forces and intrinsic surface forces [18–24]. In this paper, our model based on energy minimization is aimed to capture the key governing parameters of the deformation of the Au/PC bilayer (or the PC monolayer) at equilibrium, rather than deciphering the dynamic interfacial delamination process, which is expected to be complicated in nature. We set the total free energy of the configuration of an Au/PC bilayer (or a PC monolayer) remaining flat and suspended over a PC trench (e.g. figure 1(a)) to be zero. Therefore, the total free energy of the configuration of the Au/PC bilayer (or the PC monolayer) deforming downward and partially adhering to the PC trench bottom (e.g. figure 1(b)) is given by

$$U_{\text{total}} = U_{\text{deformation}} - b\gamma_{\text{interface}}, \quad (1)$$

where  $U_{\text{deformation}}$  denotes the strain energy of the Au/PC bilayer (or the PC monolayer) due to partial adherence deformation,  $b$  is the width of adhered portion of the PC film, and  $\gamma_{\text{interface}}$  is the interfacial adhesion between the thin PC film and the PC substrate. Given the large thickness difference between the Au/PC bilayer (or the PC monolayer) and the PC substrate, the resulting distortion deformation in the PC trench bottom is negligible, thus is not considered in computing the total free energy. If  $U_{\text{total}} > 0$ , the Au/PC bilayer (or the PC monolayer) assumes a flat morphology and remains suspended over the trench. If  $U_{\text{total}} < 0$ , the Au/PC bilayer (or the PC monolayer) prefers to deform downward and partially adhere to the trench bottom (e.g. the configuration in figure 1(b) is energetically more favorable than that in figure 1(a)).

We next compute  $U_{\text{deformation}}$  of the Au/PC bilayer due to its deformation. The result can be then readily reduced to the case of a PC monolayer. Given the large width/thickness ratio,  $a/(t_{Au} + t_{PC})$ , of the Au/PC bilayer as well as the width/depth ratio,  $a/h$ , of the trench, it is reasonable to assume the deformation of the Au/PC bilayer to be elastic. Given the large length/width ratio of the trenches, it is also

justified to assume the Au/PC bilayer to deform under the plane strain conditions (in  $x$ - $z$  plane). The  $U_{\text{deformation}}$  consists of the contributions from out-of-plane bending and in-plane stretching of the suspended portion of the Au/PC bilayer, that is

$$U_{\text{deformation}} = U_{\text{bending}} + U_{\text{stretch}}. \quad (2)$$

Assuming the out-of-plane deflection of the Au/PC bilayer to be  $w(x)$ , the resulting bending energy is given by

$$U_{\text{bending}} = \int_0^{\frac{a-b}{2}} D_{\text{Au/PC}} \left( \frac{\partial^2 w}{\partial x^2} \right)^2 dx \quad (3)$$

where  $D_{\text{Au/PC}}$  is the bending rigidity of the Au/PC bilayer and defined as [25]

$$D_{\text{Au/PC}} = \frac{(\bar{E}_{\text{Au}} t_{\text{Au}}^2 - \bar{E}_{\text{PC}} t_{\text{PC}}^2)^2 + 4\bar{E}_{\text{PC}} t_{\text{PC}} \bar{E}_{\text{Au}} t_{\text{Au}} (t_{\text{PC}} + t_{\text{Au}})^2}{12(\bar{E}_{\text{PC}} t_{\text{PC}} + \bar{E}_{\text{Au}} t_{\text{Au}})}, \quad (4)$$

in which  $\bar{E}_{\text{PC}} = E_{\text{PC}}/(1 - \nu_{\text{PC}}^2)$  and  $\bar{E}_{\text{Au}} = E_{\text{Au}}/(1 - \nu_{\text{Au}}^2)$  are the plane strain moduli of the PC and Au films, respectively. Here,  $E_{\text{PC}}$ ,  $\nu_{\text{PC}}$ ,  $E_{\text{Au}}$ ,  $\nu_{\text{Au}}$  are the Young's Modulus and Poisson's ratio of the PC and Au films, respectively.

The deformed shape of the suspended portion of the Au/PC bilayer in figure 4,  $w(x)$ , is taken to be described by a cubic polynomial of  $x$  [26], whose coefficients can be determined by the following boundary conditions:  $w = 0$  and  $dw/dx = 0$  at  $x = 0$ , and  $w = -h$  and  $dw/dx = 0$  at  $x = (a - b)/2$ . This consideration leads to

$$w(x) = 4h \left[ 4 \left( \frac{x}{(a-b)} \right)^3 - 3 \left( \frac{x}{(a-b)} \right)^2 \right]. \quad (5)$$

Substituting equation (5) into equation (3), one gets

$$U_{\text{bending}} = \frac{48D_{\text{Au/PC}}h^2}{(a-b)^3}. \quad (6)$$

The in-plane stretching energy is given by

$$U_{\text{stretch}} = \int_0^{\frac{a-b}{2}} \left( \frac{E_{\text{PC}} t_{\text{PC}}}{1 - \nu_{\text{PC}}^2} + \frac{E_{\text{Au}} t_{\text{Au}}}{1 - \nu_{\text{Au}}^2} \right) \varepsilon_{xx}^2 dx, \quad (7)$$

where  $\varepsilon_{xx}$  is the in-plane membrane strain in the Au/PC bilayer. At the equilibrium morphology, in-plane shear stress acting on the Au/PC bilayer vanishes, which leads to a constant nonzero membrane strain  $\varepsilon_{xx}$  in the suspended portion of the Au/PC bilayer. That is,

$$\varepsilon_{xx} = \frac{du}{dx} + \frac{1}{2} \left( \frac{dw}{dx} \right)^2 = \text{constant} \quad (8)$$

where  $u(x)$  is the in-plane displacement of the Au/PC bilayer in the  $x$ -direction. The symmetric configuration also requires the boundary conditions of  $u(0) = u(\frac{a-b}{2}) = 0$ . The above consideration leads to

$$\varepsilon_{xx} = \frac{12h^2}{5(a-b)^2}. \quad (9)$$

Substituting equation (9) into equation (7), one gets

$$U_{\text{stretch}} = \frac{36E_{\text{PC}}t_{\text{PC}}h^4}{25(a-b)^3(1-\nu_{\text{PC}}^2)} + \frac{36E_{\text{Au}}t_{\text{Au}}h^4}{25(a-b)^3(1-\nu_{\text{Au}}^2)}. \quad (10)$$

To compare the contribution of stretching and bending energies in the strain energy of the Au/PC layer, we compute

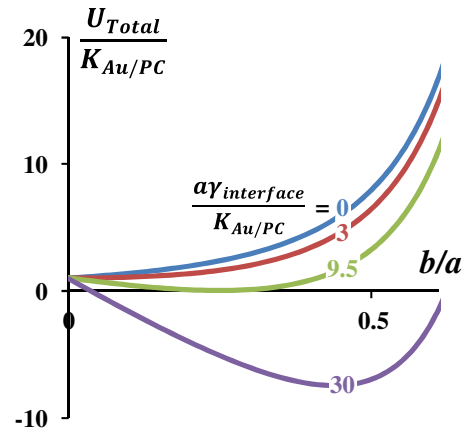


Figure 5. Normalized total free energy as a function of  $b/a$  for various values of normalized interfacial adhesion.

Table 1. Materials properties and geometric parameters.

Material properties	Geometric parameters
$E_{\text{PC}} = 2.2$ Gpa	$h = 8$ $\mu\text{m}$
$\nu_{\text{PC}} = 0.31$	$t_{\text{Au}} = 30$ nm
$E_{\text{Au}} = 79$ Gpa	$t_{\text{PC}} = 900$ nm
$\nu_{\text{Au}} = 0.44$	$a = 4$ $\mu\text{m}$ – $2000$ $\mu\text{m}$

$U_{\text{stretch}}/U_{\text{bending}}$  using equations (6) and (10). Using the parameters in our experiments (table 1), such a ratio is 19.9, indicating stretching is the dominant deformation.

Substituting equations (6) and (10) into equation (2), and then into equation (1), one gets

$$U_{\text{Total}} = \frac{48D_{\text{Au/PC}}h^2}{(a-b)^3} + \frac{36E_{\text{PC}}t_{\text{PC}}h^4}{25(a-b)^3(1-\nu_{\text{PC}}^2)} + \frac{36E_{\text{Au}}t_{\text{Au}}h^4}{25(a-b)^3(1-\nu_{\text{Au}}^2)} - b\gamma_{\text{interface}}, \quad (11)$$

or in normalized form

$$\frac{U_{\text{Total}}}{K_{\text{Au/PC}}} = \frac{1}{\left(1 - \left(\frac{b}{a}\right)\right)^3} - \frac{\alpha\gamma_{\text{interface}}}{K_{\text{Au/PC}}} \left(\frac{b}{a}\right), \quad (12)$$

where  $K_{\text{Au/PC}} = h^2 \left( \frac{48D_{\text{Au/PC}}}{a^3} + \frac{36E_{\text{PC}}t_{\text{PC}}h^2}{25a^3(1-\nu_{\text{PC}}^2)} + \frac{36E_{\text{Au}}t_{\text{Au}}h^2}{25a^3(1-\nu_{\text{Au}}^2)} \right)$ .

For the case of PC monolayer deforming and adhering partially on the trench bottom, the resulting total free energy can be readily obtained by setting  $t_{\text{Au}} = 0$  in the above derivation, which leads to a normalized form of

$$\frac{U_{\text{Total}}}{K_{\text{PC}}} = \frac{1}{\left(1 - \left(\frac{b}{a}\right)\right)^3} - \frac{\alpha\gamma_{\text{interface}}}{K_{\text{PC}}} \left(\frac{b}{a}\right), \quad (13)$$

where  $K_{\text{PC}} = h^2 \left( \frac{48D_{\text{PC}}}{a^3} + \frac{36E_{\text{PC}}t_{\text{PC}}h^2}{25a^3(1-\nu_{\text{PC}}^2)} \right)$  and  $D_{\text{PC}} = \frac{E_{\text{PC}}t_{\text{PC}}^3}{12(1-\nu_{\text{PC}}^2)}$ .

Similarly,  $U_{\text{stretch}}/U_{\text{bending}}$  for the case of PC monolayer is shown to be 25.7, also indicating stretching is the dominant deformation.

Figure 5 plots the normalized total free energy of  $\frac{U_{\text{Total}}}{K_{\text{Au/PC}}}$  as a function of  $b/a$ , for various values of dimensionless parameter  $\frac{\alpha\gamma_{\text{interface}}}{K_{\text{Au/PC}}}$ . Values of material properties and geometric parameters are listed in table 1. If the trench is narrow or the PC/PC interfacial adhesion is weak (e.g.  $\frac{\alpha\gamma_{\text{interface}}}{K_{\text{Au/PC}}} \leq 3$ ),  $\frac{U_{\text{Total}}}{K_{\text{Au/PC}}}$  increases monotonically as  $b/a$ , and is always greater

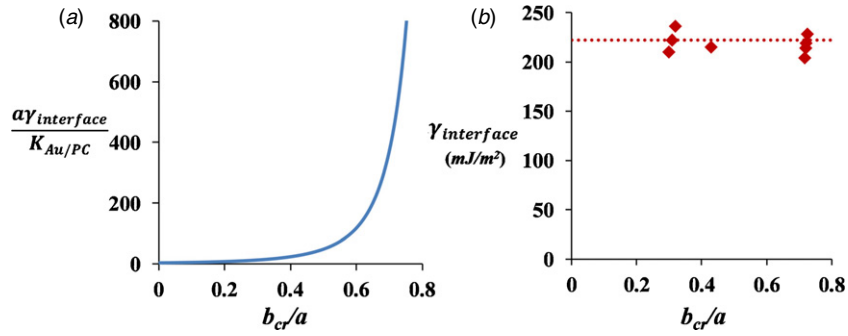


**Figure 6.** (a)  $\frac{\alpha\gamma_{\text{interface}}}{K_{\text{Au/PC}}}$  as a function of  $\frac{b_{\text{cr}}}{a}$ . For a given measurement of the width of partially adhered portion (i.e.  $b_{\text{cr}}$ ) from the sample, a value of  $\gamma_{\text{interface}}$  can be obtained from the curve in (a). Values of  $\gamma_{\text{interface}}$  obtained from measurements  $b_{\text{cr}}$  at multiple locations in both samples 1 and 2 are plotted in (b), which show an average value of  $\gamma_{\text{interface}} = 222 \text{ mJ m}^{-2}$ , with a relative standard deviation of 7.3%.

than zero. That is, the Au/PC bilayer tends to remain flat. For  $3 \leq \frac{\alpha\gamma_{\text{interface}}}{K_{\text{Au/PC}}} \leq 9.5$  (e.g. an intermediate trench width or PC/PC interfacial adhesion),  $\frac{U_{\text{Total}}}{K_{\text{Au/PC}}}$  minimizes at a finite value of  $b/a$  but is always greater than zero. In other words, the Au/PC bilayer may deform downward and partially adhere to the trench bottom to minimize the total free energy, but such a state is meta-stable since the total free energy is still higher than that if the Au/PC bilayer remains flat over the trench. When the trench is sufficiently wide or the PC/PC interfacial adhesion is strong (e.g.  $\frac{\alpha\gamma_{\text{interface}}}{K_{\text{Au/PC}}} > 9.5$ ),  $\frac{U_{\text{Total}}}{K_{\text{Au/PC}}}$  minimizes to reach a negative value at a finite value of  $b/a$ . That is, the Au/PC bilayer tends to deform downward and partially adhere to the trench bottom.

The critical value of  $\frac{b_{\text{cr}}}{a}$  corresponding to the minimum total free energy when the Au/PC layer tends to deform downward and partially adhere to the trench bottom can be determined by setting  $\partial\left(\frac{U_{\text{Total}}}{K_{\text{Au/PC}}}\right)/\partial(b/a) = 0$ , which leads to

$$\frac{3}{\left(1 - \frac{b_{\text{cr}}}{a}\right)^4} = \frac{\alpha\gamma_{\text{interface}}}{K_{\text{Au/PC}}}. \quad (14)$$

Figure 6(a) plots  $\frac{\alpha\gamma_{\text{interface}}}{K_{\text{Au/PC}}}$  as a function of  $\frac{b_{\text{cr}}}{a}$ . It shows that, for a given trench width  $a$ , the wider the portion adhered to the trench bottom, the stronger the interfacial adhesion between the thin PC layer and the PC substrate. The intersection of the curve with the axis (i.e.  $\frac{b_{\text{cr}}}{a} = 0$ ) defines a critical value of  $\frac{\alpha\gamma_{\text{interface}}}{K_{\text{Au/PC}}} = 3$ , below which the Au/PC bilayer remains flat over the trench. As discussed above, only when  $\frac{\alpha\gamma_{\text{interface}}}{K_{\text{Au/PC}}} > 9.5$ , the Au/PC bilayer can stably deform downward and partially adhere to the trench bottom.

Note that for the case of PC monolayer deforming downward, its total free energy (equation (13)) assumes the same form as that for the case of Au/PC bilayer (equation (12)). Therefore, the results in figures 5 and 6(a) and in equation (14) are also valid for the case of PC monolayer, by just replacing  $K_{\text{Au/PC}}$  with  $K_{\text{PC}}$ .

Equation (14) can then be used to quantitatively determine the interfacial adhesion between the thin PC layer and the PC substrate by measuring  $b_{\text{cr}}$ , the width of partially adhered portion of the Au/PC bilayer (or the PC monolayer) over a sufficiently wide trench from the samples (e.g. figures 3(e) and (f)). For example, for the Au/PC bilayer over a  $200 \mu\text{m}$  wide trench, figure 3(e) gives  $b_{\text{cr}}/a = 0.33$ , which leads to  $\gamma_{\text{interface}} =$

$251 \text{ mJ m}^{-2}$ , and over a  $500 \mu\text{m}$  wide trench, figure 3(f) gives  $b_{\text{cr}}/a = 0.71$ , which leads to  $\gamma_{\text{interface}} = 204 \text{ mJ m}^{-2}$ . For the PC monolayer over a  $200 \mu\text{m}$  wide trench, measurement shows that  $b_{\text{cr}}/a = 0.43$ , which leads to  $\gamma_{\text{interface}} = 215 \text{ mJ m}^{-2}$ . Figure 6(b) also plots the estimated values of  $\gamma_{\text{interface}}$  from the measurements of  $b_{\text{cr}}$  at multiple locations in both sample 1 and sample 2. These estimated values average at  $\bar{\gamma}_{\text{interface}} = 222 \text{ mJ m}^{-2}$  with a relative standard deviation less than 7.3%. Such a good agreement of the estimated PC/PC interfacial adhesion based on measurements at multiple locations in samples of two different material combinations demonstrates the accuracy and robustness of our approach to determining interfacial adhesion between submicron thin films and polymer substrates. Humidity may cause the formation of a meniscus at the delaminating front of the PC/PC interface. Our measurement of the water contact angle of the PC surface is about  $94.5^\circ$ , leading to a possible variation of adhesion energy by  $\sim 11 \text{ mJ m}^{-2}$  (5% of the value of  $\bar{\gamma}_{\text{interface}}$ ). Applying  $\bar{\gamma}_{\text{interface}} = 222 \text{ mJ m}^{-2}$  to the critical conditions of  $\frac{\alpha\gamma_{\text{interface}}}{K_{\text{Au/PC}}} > 9.5$  (or  $\frac{\alpha\gamma_{\text{interface}}}{K_{\text{PC}}} > 9.5$ ) leads to a critical trench width of  $192 \mu\text{m}$  (or  $155 \mu\text{m}$ ), above which the Au/PC bilayer (or the PC monolayer) tends to deform and partially adhere to the trench bottom. These predictions also agree well with our experimental observations, further validating our approach to determining the interfacial adhesion of ultrathin films.

#### 4. Concluding remarks

We demonstrate a feasible and robust approach to determining the interfacial adhesion of submicron thin films by combining nTP experiments and mechanical modeling. Such an approach is motivated by the observation that a thin film (monolayer or multilayers) fabricated over a long trench via nTP may deform downward and partially adhere to the bottom of the trench if the trench width is sufficiently large. A mechanics model can then explicitly correlate the interfacial adhesion between the thin film and the trench material with the width of adhered portion of the thin film as well as the thin film mechanical properties and the trench geometry. Such an approach is applied to determine the interfacial adhesion between a submicron thick PC film and a PC substrate, which is shown to be about  $222 \text{ mJ/m}^2$ , with an agreement of measurements at multiple locations in multiple samples within

7.3%. Since the nTP process has been successfully used to fabricate multilayer thin-film structures consisting of a wide range of materials, the approach presented in this paper can be potentially extended to measure the adhesion of interfaces of other material combinations and of ultrafine length scales that are inaccessible to traditional approaches for interfacial adhesion measurement. In this sense, results from this study shed light on better understanding of the adhesive properties of functional interfaces, which in turn help guide the optimal design of MEMS and NEMS.

## Acknowledgments

This research is supported by National Science Foundation (grants # 0856540 and 0928278). The authors thank Reza Ghodssi, Brendan Hanrahan and Nathan Siwak for their help in using the Veeco interferometric microscope.

## References

- [1] Spearing S M 2000 Materials issues in microelectromechanical systems (MEMS) *Acta Mater.* **48** 179–96
- [2] Craighead H G 2000 Nanoelectromechanical systems *Science* **290** 1532–5
- [3] Ekinci K L and Roukes M L 2005 Nanoelectromechanical systems *Rev. Sci. Instrum.* **76** 061101
- [4] Yao J J 2000 RF MEMS from a device perspective *J. Micromech. Microeng.* **10** R9–38
- [5] Zhao Y P, Wang L S and Yu T X 2003 Mechanics of adhesion in MEMS—a review *J. Adhes. Sci. Technol.* **17** 519–46
- [6] Mastrangelo C H 1997 Adhesion-related failure mechanisms in micromechanical devices *Tribol. Lett.* **3** 223–38
- [7] Maboudian R and Howe R T 1997 Critical review: adhesion in surface micromechanical structures *J. Vac. Sci. Technol. B* **15** 1–20
- [8] Loo Y L, Willett R L, Baldwin K W and Rogers J A 2002 Interfacial chemistries for nanoscale transfer printing *J. Am. Chem. Soc.* **124** 7654–5
- [9] Zaumseil J *et al* 2003 Three-dimensional and multilayer nanostructures formed by nanotransfer printing *Nano Lett.* **3** 1223–7
- [10] Hines D R *et al* 2005 Nanotransfer printing of organic and carbon nanotube thin-film transistors on plastic substrates *Appl. Phys. Lett.* **86** 163101
- [11] Feng X, Meitl M A, Bowen A M, Huang Y, Nuzzo R G and Rogers J A 2007 Competing fracture in kinetically controlled transfer printing *Langmuir* **23** 12555–60
- [12] Tucker M B, Hines D R and Li T 2009 A quality map of transfer printing *J. Appl. Phys.* **106** 103504
- [13] Chanda D *et al* 2011 Large-area flexible 3D optical negative index metamaterial formed by nanotransfer printing *Nature Nanotechnol.* **6** 402–7
- [14] Chen J H, Ishigami M, Jang C, Hines D R, Fuhrer M S and Williams E D 2007 Printed graphene circuits *Adv. Mater.* **19** 3623–7
- [15] Hines D R, Ballarotto V W, Williams E D, Shao Y and Solin S A 2007 Transfer printing methods for the fabrication of flexible organic electronics *J. Appl. Phys.* **101** 024503
- [16] Ahn J H *et al* 2006 Heterogeneous three-dimensional electronics by use of printed semiconductor nanomaterials *Science* **314** 1754–7
- [17] Dechaumphai E, Zhang Z, Siwak N P, Ghodssi R and Li T 2010 Resonant frequency of gold/polycarbonate hybrid nano resonators fabricated on plastics via nano-transfer printing *Nanoscale Res. Lett.* **6** 90
- [18] Wan K T 1999 Fracture mechanics of a V-peel adhesion test—transition from a bending plate to a stretching membrane *J. Adhes.* **70** 197–207
- [19] Wan K T and Duan J 2002 Adherence of a rectangular flat punch onto a clamped plate: transition from a rigid plate to a flexible membrane *Trans. ASME, J. Appl. Mech.* **69** 104–9
- [20] Yang F Q 2004 Contact deformation of a micromechanical structure *J. Micromech. Microeng.* **14** 263–8
- [21] Wong M F, Duan G and Wan K T 2007 Adhesion-delamination mechanics of a prestressed rectangular film adhered onto a rigid substrate *J. Appl. Phys.* **101** 024903
- [22] Li G X and Wan K T 2010 Delamination mechanics of a clamped rectangular membrane in the presence of long-range intersurface forces: transition from JKR to DMT limits *J. Adhes.* **86** 335–51
- [23] Lu Z X and Dunn M L 2010 van der Waals adhesion of graphene membranes *J. Appl. Phys.* **107** 044301
- [24] Duan G and Wan K T 2010 ‘Pull-in’ of a pre-stressed thin film by an electrostatic potential: A 1D rectangular bridge and a 2D circular diaphragm *Int. J. Mech. Sci.* **52** 1158–66
- [25] Gay D, Hoa S V and Tsai S W 2003 *Composite Materials: Design and Applications* (Boca Raton, FL: CRC Press)
- [26] Zhang Z and Li T 2010 Graphene morphology regulated by nanowires patterned in parallel on a substrate surface *J. Appl. Phys.* **107** 103519